In the last lecture, for magnetic resonance, we introduced the concept of "observation from rotating coordinates" . The time evolution of the angular momentum was treated in the Heisenberg picture, and the results were the same as that obtained in the classical picture as in eq. (2.83). Then in the following, for simplicity, we consider classical equations of motion for macroscopic magnetic moment $\boldsymbol{M}$ and introduce energy and phase relaxations phenomenologically[1].

$$\frac{dM_z}{dt} = \gamma[\boldsymbol{M}\times\boldsymbol{H}]_z + \frac{M_0 - M_z}{T_1}, \tag{2.89a}$$

$$\frac{dM_{x,y}}{dt} = \gamma[\boldsymbol{M}\times\boldsymbol{H}]_{x,y} - \frac{M_{x,y}}{T_2}. \tag{2.89b}$$

T_1, T_2 are longitudinal and transverse relaxation times respectively, or energy and phase relaxation times. We here use $\boldsymbol{H}$ instead of $\boldsymbol{B}$ to avoid confusion due to the existence of $\boldsymbol{M}$ though the use of $\boldsymbol{B}$ is not the problem at all. The definition of gyromagnetic ratio should be changed from eq. (2.14) so as to have consistent dimension. We consider a static field $\boldsymbol{H}_0$ along z and a rotating field $\boldsymbol{H}_1/2$ in xy-plane with an angular frequency $(-)\omega$. The total field is

$$\boldsymbol{H} = (\frac{H_1}{2}\cos\omega t, -\frac{H_1}{2}\sin\omega t, H_0). \tag{2.90}$$

The magnetic moment derived from the angular momentum gets minus sign due to the sign of electric charge (eq. (1.80)). Hence the rotation is clockwise for positive magnetic moment $\boldsymbol{M}$. The equations of motion are thus,

$$\frac{dM_x}{dt} = \gamma[M_y H_0 + M_z\frac{H_1}{2}\sin\omega t] - \frac{M_x}{T_2}, \tag{2.91a}$$

$$\frac{dM_y}{dt} = \gamma[M_z\frac{H_1}{2}\cos\omega t - M_x H_0] - \frac{M_y}{T_2}, \tag{2.91b}$$

$$\frac{dM_z}{dt} = \gamma[-M_x H_1\sin\omega t - M_y\frac{H_1}{2}\cos\omega t] + \frac{M_0 - M_z}{T_1}. \tag{2.91c}$$

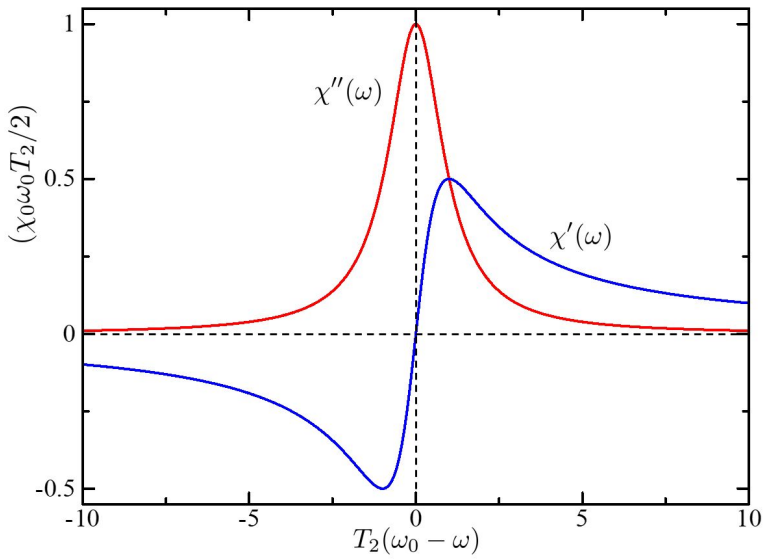

Fig. 2.14 The plot of eq. (2.96). The real part ($\chi'(\omega)$, blue line) and the imaginary part ($\chi''(\omega)$, red line) of the complex susceptibility around a magnetic resonance in the presence of relaxations.

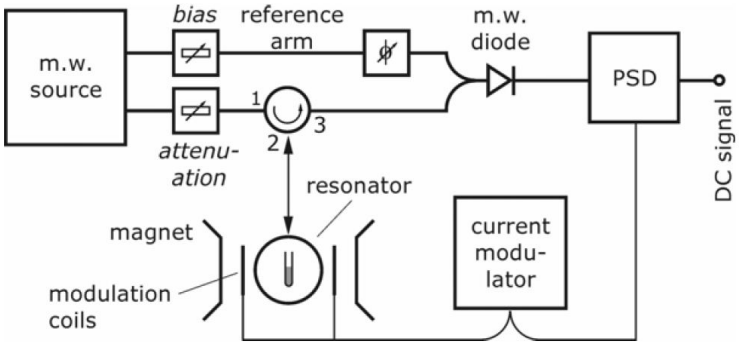

Fig. 2.15 Typical setup of electron paramagnetic resonance (electron spin resonance) experiment.The circle mark with numbering indicates a circulator of microwave. A microwave enters via terminal 1 through 2 to the cavity with a sample and the reflected wave propagates through 3 to a diode. The detected signal is sent to a phase sensitive detector (PSD). From [2].

We introduce the coordinate system (x', y', z') $(z' = z)$ rotating around z-axis clockwise with angular frequency ω to obtain

$$M_{x'} = M_x \cos\omega t - M_y \sin\omega t, \tag{2.92a}$$
$$M_{y'} = M_x \sin\omega t + M_y \cos\omega t. \tag{2.92b}$$

By using eq. (2.92), we rewrite eq. (2.91) into the kinetic equations of $(M_{x'}, M_{y'}, M_z)$. Under the conditions:

$$\begin{aligned} &\frac{dM_{x'}}{dt} = \frac{dM_{y'}}{dt} = 0 \quad \text{(stationary state)}, \\ &M_z \simeq M_0 = \chi_0 H_0 \quad \text{(oblique angle is small)}, \end{aligned} \tag{2.93}$$

we obtain the following solutions.

$$M_{x'} = \chi_0\omega_0 T_2 \frac{(\omega_0 - \omega)T_2 H_1/2}{1 + (\omega_0 - \omega)^2 T_2^2 + \gamma^2 (H_1/2)^2 T_1 T_2} \tag{2.94a}$$
$$M_{y'} = \chi_0\omega_0 T_2 \frac{H_1/2}{1 + (\omega_0 - \omega)^2 T_2^2 + \gamma^2 (H_1/2)^2 T_1 T_2}. \tag{2.94b}$$

ω_0 is Larmor frequency ω_{L} in eq. (2.86) with $B = \mu_0 H_0$.

The solution expresses a state with a comparatively large relaxation, thus the moment gets large friction in rotation around $\boldsymbol{H}_1$. Hence the stationary state has a small angle to z-axis. From the rest system,

$$M_x = \chi'(\omega) H_1 \cos\omega t + \chi''(\omega) H_1 \sin\omega t, \tag{2.95a}$$
$$M_y = -\chi'(\omega) H_1 \sin\omega t + \chi''(\omega) H_1 \cos\omega t. \tag{2.95b}$$

In case $\gamma^2 H_1^2 T_1 T_2 \ll 1$ (large relaxation), the real and imaginary parts of the susceptibility are given by

$$\chi'(\omega) = \frac{\chi_0\omega_0}{2} T_2 \frac{(\omega_0 - \omega)T_2}{1 + (\omega_0 - \omega)^2 T_2^2}, \tag{2.96a}$$
$$\chi''(\omega) = \frac{\chi_0\omega_0}{2} T_2 \frac{1}{1 + (\omega_0 - \omega)^2 T_2^2}, \tag{2.96b}$$

respectively, that is $\chi = \chi' - i\chi''$. They are plotted against $\omega_0 - \omega$ in Fig. 2.14.

In the experiments, the specimens are placed in coils or cavities of resonators and the variations of resonance characteristics are detected. An increase in energy dissipation in a resonator results in a widening and lowering of the resonance peak [*1]. Figure 2.15 illustrates a typical setup of experiments. A microwave enters via terminal 1 through 2 to the cavity with a sample and the reflected wave propagates through 3 to a three port connection for interference and then to a detector (diode). The signal is then sent to a phase sensitive detector (PSD). Variation of resonant frequency in microwave cavity is not so easy in most cases, so usually it is fixed. The frequency of input microwave is tuned to the resonance.

[*1] This can be understood, e.g, by inserting a resistor into an LC resonator circuit in a model for calculation.

Instead, the Larmor frequency $\omega_{\rm L}$ in eq. (2.86) of the sample is swept by the external magnetic field. In eq. (2.96), this corresponds to the variation of ω_0, and anyway the resonance curve is obtained. ω_0 in the coefficients of eq. (2.96) gives the first order slow variation while the resonance generally has a sharp lineshape and the distortion due to the coefficient is ignorable. The imaginary part in eq. (2.96), $\chi'(\omega)$ (eq. (2.96b)) represents the energy dissipation, which shows a peak structure as the red line in Fig. 2.14.

Coils for the field modulation is drawn in Fig. 2.15. In many experiments, field modulation with frequencies around 100 kHz is applied for improvement of signal to noise ratio by taking PSD signal. Such signals appear as frequency-derivative of eq. (2.96b).

2.9.2 Hyperfine structures in electron paramagnetic resonance

Owing to the large magnetic moment of electrons, electron spin resonance (ESR)or electron paramagnetic resonance (EPR)has high sensitivities among various magnetic resonance. Atomic wavefunctions of electron have finite amplitudes in the neighbors of nucleuses. When a nucleus has a finite spin, the exchange interaction (which will be introduced later) between the nuclear spin $\boldsymbol{I}$ and the electron total angular momentum $\boldsymbol{J}$ brings about **hyperfine interaction**, which can be expressed as

$$\mathcal{H}_{\rm HF} = A\boldsymbol{I}\cdot\boldsymbol{J}. \tag{2.97}$$

A is a parameter of the strength in the interaction. Since the Hamiltonian in eq. (2.97) has the same form as the spin-orbit interaction eqs. (2.38), (2.39), we consider the total angular momentum $\boldsymbol{F} = \boldsymbol{I}+\boldsymbol{J}$, and write the simultaneous eigenstate of $\mathcal{H}$, $\boldsymbol{F}^2$, F_z as $|F, M_F\rangle$. Then just as eq. (2.41), the eigenvalue of $\mathcal{H}_{\rm HF}$ is given by

$$\mathcal{H}_{\rm HF}|F,M_F\rangle = A\frac{\boldsymbol{F}^2-\boldsymbol{I}^2-\boldsymbol{J}^2}{2}|F,M_F\rangle = A\frac{F(F+1)-I(I+1)-J(J+1)}{2}|F,M_F\rangle. \tag{2.98}$$

The naming of "hyperfine" interaction comes from the further splitting of absorption levels, that already split by $\mathcal{H}_{\rm SOI}$. We do not have enough time to go into very important field and I recommend the readers who have strong interest in this field to refer to the journal "Hyperfine Interactions" [*2] .

2.9.3 Electron paramagnetic resonance in paramagnetic salts

EPRs are flourishing in the paramagnetic salts that have $3d$ transition metals or $4f$ lanthanoids as sources of magnetic moments. They have comparatively high moment densities (depending on the impurity concentrations), and importantly they are insulating that allows high frequency electromagnetic wave to go into the bulk in the absence of the skin effect.

Here we introduce an example of analyzing EPR data. Because EPR not only is sensitive but also has high resolution bringing rich information on the localized electronic states. For the actual analysis, we thus need a higher order approximation. In the case of $3d$ transition metals, we have discussed that the effect of orbital angular moment disappears due to the strong effect of ligand fields. Conversely, in $4f$ lanthanoid, we have given the priority to the spin-orbit interaction. However, these are the first order approximation and in the next step, we need to consider the SOI in the former, and the crystal field splitting in the latter. We skip the hyperfine interaction, which is not important for nucleus without spin, but consideration of the SOI on crystal field split levels is indispensable. For that we introduce the concept of effective spin Hamiltonian, which is common in this field. The effective spin Hamiltonian has no orbital operator but gives the same answer as the original one, if we restrict the problem to the effect of the SOI on the orbital levels that diagonalize the crystal field Hamiltonian[3].

[*2] https://www.springer.com/journal/10751

Let $\{\varphi_0, \varphi_1, \cdots, \}$ be an orbital basis that diagonalizes $\mathcal{H}_{\rm orb} = \mathcal{H}_0 + \mathcal{H}_{\rm CF}$, and in ket format $|n\rangle_{\rm o}$. We write the energy eigenvalues as ${}_{\rm o}\langle n|\mathcal{H}_{\rm orb}|n'\rangle_{\rm o} = E_n\delta_{nn'}$, the total spin of the basis as S, the spin wavefunction as $\{\phi_{-2S}, \phi_{-2S+1}, \cdots, \phi_{2S}\}$, ket-expression $|m\rangle_{\rm s}$.

The perturbation Hamiltonian of the SOI and the Zeeman effect is

$$\mathcal{H}' = \lambda \boldsymbol{L}\cdot\boldsymbol{S} + \mu_{\rm B}(\boldsymbol{L} + g_{\rm e}\boldsymbol{S})\cdot\boldsymbol{H}, \tag{2.99}$$

where $g_{\rm e}$ is g-factor of electron. We write a wavefunction in an expanded form as

$$\Psi = \sum_{nm} a_{nm}\varphi_n\phi_m = \sum_{nm} a_{nm}|n\rangle_{\rm o}|m\rangle_{\rm s}. \tag{2.100}$$

Then the eigenvalue equation of the total Hamiltonian is

$$\mathcal{H}\Psi = (\mathcal{H}_{\rm orb} + \mathcal{H}')\Psi = E\Psi. \tag{2.101}$$

Here e.g., the orbital part is integrated out in ${}_{\rm o}\langle l|\mathcal{H}'|n\rangle_{\rm o}$ but this still has the spin part as operator(s). Then we define a spin Hamiltonian as a second-order perturbation formula, in which the orbital part is integrated out. If the unperturbed ground state has degeneracy, we change the basis according to the perturbation theory, but there should be no confusion in using the symbols like $|n\rangle_{\rm o}$. We also restrict the transition matrix elements to the ones with the ground state $|0\rangle_{\rm o}$. Thus we obtain [*3]

$$\tilde{\mathcal{H}} = {}_{\rm o}\langle 0|\mathcal{H}'|0\rangle_{\rm o} + \sum_{n\neq 0}\frac{{}_{\rm o}\langle 0|\mathcal{H}'|n\rangle_{\rm o}\,{}_{\rm o}\langle n|\mathcal{H}'|0\rangle_{\rm o}}{E_0 - E_n}. \tag{2.102}$$

The introduction of ligand field quenches the orbital angular momentum. Namely the diagonal terms vanish ${}_{\rm o}|0|\boldsymbol{L}|0\rangle_{\rm o} = 0$ to give

$${}_{\rm o}\langle 0|\mathcal{H}'|0\rangle_{\rm o} = g_{\rm e}\mu_{\rm B}\boldsymbol{S}\cdot\boldsymbol{H}. \tag{2.103}$$

In the same way, from

$${}_{\rm o}\langle 0|\mathcal{H}'|n\rangle_{\rm o} = {}_{\rm o}|0|\boldsymbol{L}|n\rangle_{\rm o}\cdot(\lambda\boldsymbol{S} + \mu_{\rm B}\boldsymbol{H}), \tag{2.104}$$

we obtain

$$\tilde{\mathcal{H}} = g_{\rm e}\mu_{\rm B}\boldsymbol{S}\cdot\boldsymbol{H} - (\lambda\boldsymbol{S} + \mu_{\rm B}\boldsymbol{H})\Lambda(\lambda\boldsymbol{S} + \mu_{\rm B}\boldsymbol{H}), \tag{2.105}$$

where Λ is a tensor given by

$$\Lambda_{ij} = \sum_{n\neq 0}\frac{{}_{\rm o}\langle 0|L_i|n\rangle_{\rm o}\,{}_{\rm o}\langle n|L_j|0\rangle_{\rm o}}{E_n - E_0} \quad (i,j = x,y,z). \tag{2.106}$$

These elements are not necessarily zero and the effect of spin-orbit interaction appears in the second order perturbation. The same view is given by considering that the vanishing expectation value of orbital angular momentum comes from the way of superposition and the cancellation does not work for off-diagonal elements. Equation (2.105) is expanded as

$$\tilde{\mathcal{H}} = \mu_{\rm B}\boldsymbol{S}g_{\rm e}(\mathbf{1} - \lambda\Lambda)\boldsymbol{H} - \lambda^2\boldsymbol{S}\Lambda\boldsymbol{S} - \mu_{\rm B}^2\boldsymbol{H}\Lambda\boldsymbol{H}. \tag{2.107}$$

The first term is written in the Zeeman form as

$$\tilde{\boldsymbol{g}} = g_{\rm e}(\mathbf{1} - \lambda\Lambda). \tag{2.108}$$

This is an expansion of g-factor to a tensor form. Taking the principal axes of the tensor to x, y, z, we can write the second term in the following form.

$$-\lambda^2\boldsymbol{S}\Lambda\boldsymbol{S} = D\left[S_z^2 - \frac{S(S+1)}{3}\right] + E(S_x^2 - S_y^2), \tag{2.109}$$

[*3] You may not be satisfied with this treatment. In that case refer to a tutorial review [4]. A textbook in Japanese [5] gives rigorous treatment based on the projection operator method.

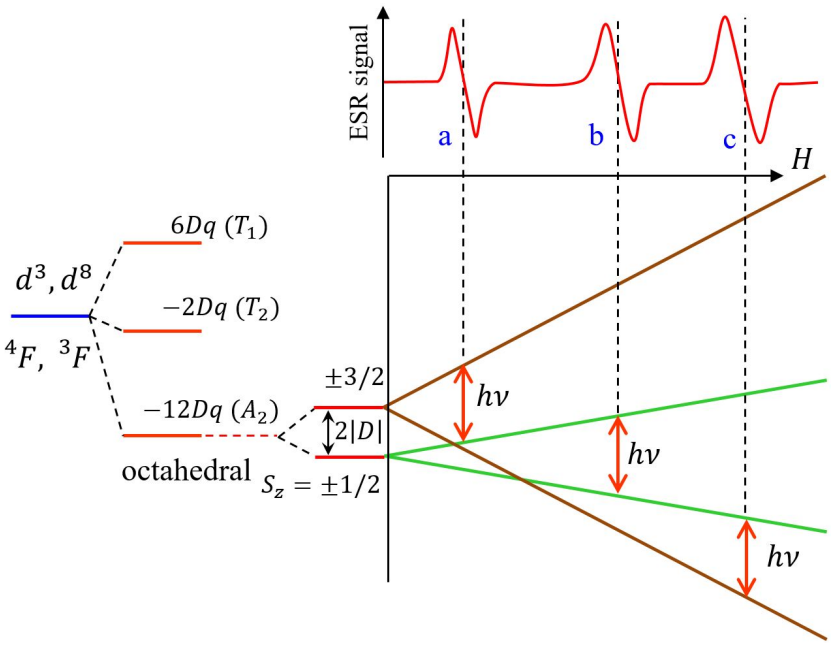

Fig. 2.16 Level splitting of $Cr^{3+}(3d^3$, S=3/2) in weak crystal field approximation and Zeeman splitting by external field. E=0 is assumed. Expected three ESR peak signals for microwave frequency ν corresponding to the red arrows are illustrated.

where Λ determines coefficients D and E in proportion to λ^2, called axial and orthorhombic coefficients respectively [*4]. The third term does not cause level-splitting being a small effect of orbital magnetic moment induced by external field. With dropping this term we reach

$$\tilde{\mathcal{H}} = \mu_{\mathrm{B}} \boldsymbol{S}\tilde{\boldsymbol{g}}\boldsymbol{H} + D\left[S_z^2 - \frac{S(S+1)}{3}\right] + E(S_x^2 - S_y^2). \tag{2.110}$$

As a simple example, let $\tilde{\boldsymbol{g}}$ be isotropic, $E = 0$, and $S = 3/2$. The spin states active for EPR are four states of $S_z = \pm 1/2, \pm 3/2$. At $H = 0$ they degenerate into two with the distance of $2|D|$ from eq. (2.110). Figure 2.16 illustrates such situation. The LS multiplet $(3d)^3$ is split as in the figure in weak field approximation given in App. 5A. The ground

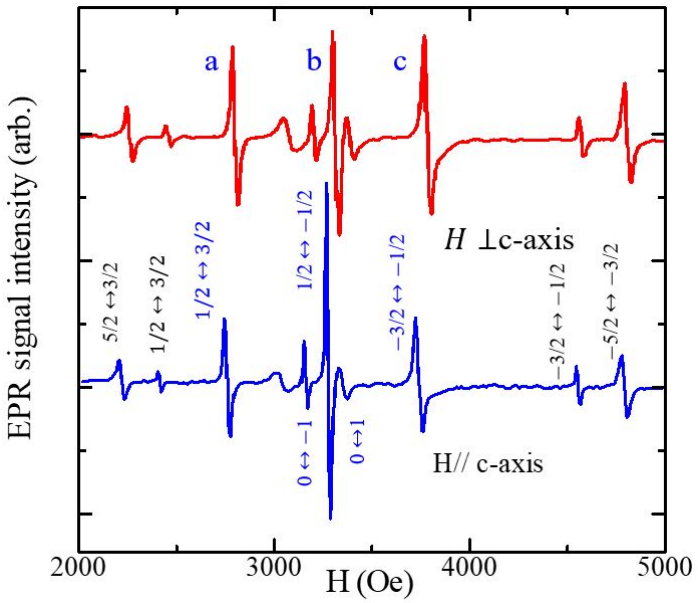

Fig. 2.17 EPR spectra of $BaTiO_3$ doped with 1% Cr^{3+} and Fe^{3+}. Blue and red lines are data for magnetic field parallel and perpendicular to c-axis respectively. The data are offset for clarity. Peaks (look like dissipation because of derivative taking in experiment) assigned as a, b, and c correspond to a, b, and c in Fig. 2.16. The microwave is in X-band (9-10 GHz), for which the value is not given. The annotations in blue letters indicate absorptions of S =3/2 state in Cr^{3+}, and S=1 state in Cr dimers. Those in black letters indicate absorptions of $S = 5/2$ in Fe^{3+}. From [6].

[*4] Repeated usage of D or E for different quantities inevitably causes confusion. These jargons are commonly used in many research papers and sometimes we find such symbols appear in a single diagram or table with different meanings. In this field we are often forced to express complicated concepts with simple and clear symbols, and at present we find no other better way. The readers are requested to judge from the context.

Ion	Crystal	g		$\lvert D\rvert$ (cm^{-1})	$\lvert E\rvert$ (cm^{-1})
Fe^{3+}	$BaTiO_3$	2.000		0.022	0.0079
another report		2.003		0.0987	
Cr^{3+}	$BaTiO_3$	1.975		0.046	0.0055
	h-$BaTiO_3$	H1 g_z=	1.9797	0.105	
		H1 $g_{x,y}$=	1.9857		
		H2 g_z=	1.9736	0.3220	
		H2 $g_{x,y}$=	1.9756		

Tab. 2.9 Values of g, $|D|$, $|E|$ for Fe^{3+} and Cr^{3+} in $BaTiO_3$ obtained from EPR lines in Fig. 2.17.

state is A_2 ($S = 3/2$). The external field split the two into four as in the figure. With microwave of frequency ν corresponding to the red arrows in the figure, absorptions at positions a, b, and c assuming equal populations of levels at high-enough temperatures.

Cr^{3+} (d^3, ^4F) often takes the states close to the above ideality. Figure 2.17 shows an EPR experiment on Cr^{3+}, in which they doped 1% Fe^{3+} and Cr^{3+} into cubic state of $BaTiO_3$. Three main peaks corresponding to a, b, and c in Fig. 2.16 are observed[6]. The lineshape did not change with the direction of magnetic field indicating that $\tilde{\boldsymbol{g}}$ is isotropic though finite E is deduced from the relative peak positions. The data indicate doped Cr^{3+} is in tetragonal state. The absorption peaks for $S = 1$ are from Cr dimers. The parameters are shown in Tab. 2.9.

$BaTiO_3$ also has hexiagonal phase h-$BaTiO_3$. Cr^{3+} impurities in h-$BaTiO_3$ show very different EPR absorption lines. Even this spectrum can be explained by the spin Hamiltonian of eq. (2.110) with an anisotropic $\tilde{\boldsymbol{g}}$ and parameters shown in the table[7].

2.9.4 Magnetic refrigeration

Magnetic refrigeration (MR) is a cooling method that can exert cooling ability in a wide temperature range by selecting a magnetic moment system (working substance) from room temperature to ultra-low temperature. The MR with paramagnetic salt was once main player in creating very low temperature till 1960's, then in the range from 0.01 to 1 K the position was replaced by the dilution refrigerators[8]. On the other hand, below few mK, once Pomeranchuk cooling was used, but then the main shifted to **nuclear demagnetization**.Even in regions other than low temperatures, the MR are now used for various purposes. Exploration of cooling substances spans not only paramagnetic materials but also

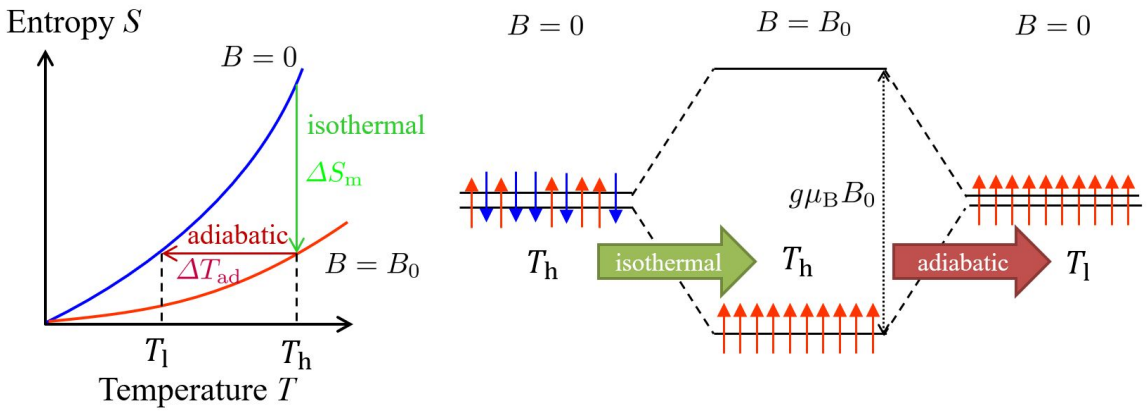

Fig. 2.18 Concept of magnetic refrigeration. Left: Illustration of temperature variation of entropy in a magnetic system in zero and finite magnetic fields. The green arrow indicates first isothermal application of magnetic field. The brown arrow shows adiabatic demagnetization. The right figure illustrates evolution of spin distribution in the sequence of isothermal field application and adiabatic demagnetization in a simple two-level spin system.

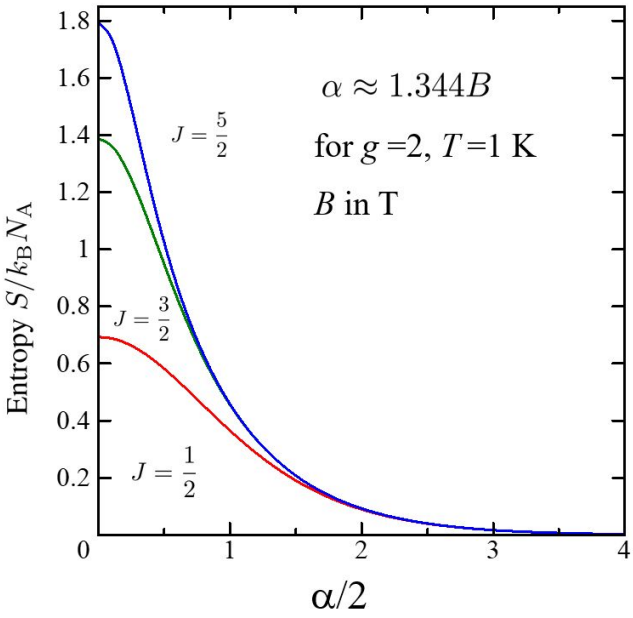

Fig. 2.19 Entropy in eq. (2.113) is expressed as a function of α for $J = 1/2, 3/2, 5/2$.

those have phase transitions caused by interactions between spins and magnetic field. In recent years, regardless of its pros and cons, the possibility of liquefying and transporting hydrogen has been explored, and development research using magnetic refrigeration for cooling is also being conducted[9].

The principle of MR is simple as follows. A free spin system has random directions in spin and the maximum entropy at zero field. With the isothermal magnetization, the spins are aligned along the magnetic field by the Zeeman effect. The process reduces the entropy. Hence a heat is discharged to the environment. Then during the adiabatic demagnetization, the entropy is kept constant. In the spin distribution, there is no increase in the population to excited states in spite of decrease in the distance between the ground and the excited states. This is a low temperature state. With connecting this coolant to a material to be cooled, a heat is transferred from this material to the coolant. The process is summarized in Fig. 2.18.

Let S be the entropy of system composed of paramagnetic ions with total angular momentum J. At zero field, $S = k_{\rm B}N_{\rm A}\ln(2J+1)$ for 1 mol. Let us write the variation in S with isothermal magnetization up to B as $\Delta S(B, T_{\rm i})$. Then with the final temperature $T_{\rm f}$ after the **adiabatic demagnetization**, $\Delta S(B, T_{\rm i})$ is given by

$$\Delta S(B, T_{\rm i}) = S(0, T_{\rm i}) - S(B, T_{\rm i}) = \int_{T_{\rm f}}^{T_{\rm i}} \frac{C_{\rm m}}{T} dT, \quad C_{\rm m} = T\left(\frac{\partial S}{\partial T}\right)_{B=0}. \tag{2.111}$$

C_m is the specific heat at zero field.

The magnetization M and the entropy S are calculated just as eq. (1.25) as

$$M = N_{\rm A} g \mu_{\rm B} \left[\frac{2J+1}{2}\coth\left(\frac{2J+1}{2}\alpha\right) - \frac{1}{2}\coth\frac{\alpha}{2}\right], \quad \alpha \equiv \frac{g\mu_{\rm B}B}{k_{\rm B}T}, \tag{2.112}$$

$$\frac{S}{N_{\rm A}k_{\rm B}} = \frac{\alpha}{2}\coth\frac{\alpha}{2} - \frac{2J+1}{2}\alpha\coth\left[\frac{2J+1}{2}\alpha\right] + \ln\left[\frac{\sinh[(2J+1)\alpha/2]}{\sinh\alpha/2}\right]. \tag{2.113}$$

Figure 2.19 shows the results for J =1/2, 3/2, 5/2. Since $\alpha \approx 1.344B$ (B in T) for $g = 2$, T =1 K, the most of entropy in a free spin system at T=1 K can be removed by cycling of B =2 T.

The spins in paramagnetic salts maintain a relatively large entropy even at low temperatures where other degrees of freedom are quenched, such as lattice vibration, so they are used to obtain extremely low temperatures based on low temperatures. However, e.g., if we choose a material with a phase transition induced by magnetic field, a large decrease in entropy is expected even at high temperatures. This can be understood by a Maxwell relation

$$\left(\frac{\partial S}{\partial B}\right)_T = \left(\frac{\partial M}{\partial T}\right)_B, \tag{2.114}$$

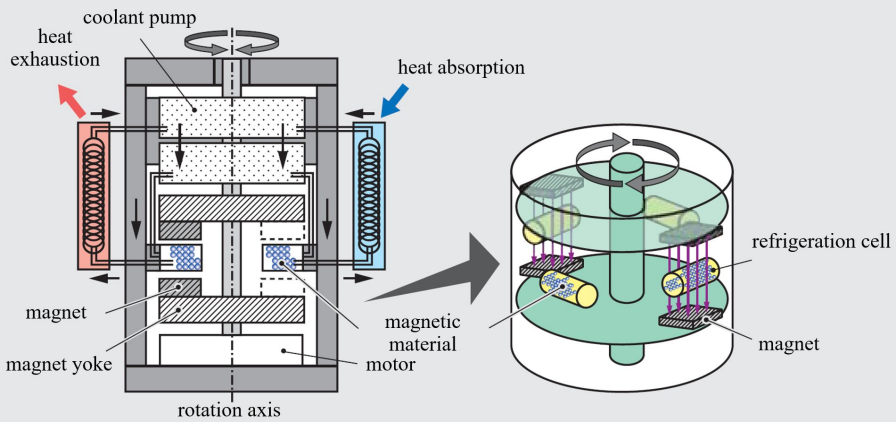

Fig. 2.20 Schematic diagram of active magnetic refrigeration (AMR). From Akiko Saito, Toshiba Review Vol.62, 78 (2007) (in Japanese).

in which magnetic field variation of entropy is proportional to temperature derivative of magnetization.

Gd (Curie temperature 289 K) is frequently used as a cooling material, which can have a cooling power at around room temperature.Further research and development of working materials and methods are underway with the aim of putting them into practical use near room temperature. For the use of MR under continuous inflow of heat, a continuous cooling method is active magnetic refrigeration (AMR) illustrated in Fig. 2.20. Magnetization/demagnetization is done by rotation of tables, to which permanent magnets are fixed. The turn table scheme realizes successive on/off of magnetic field and continuous flow of refrigerant realizes continuous cooling.

There are many proposals and exploration of cooling substance, e.g., nano-particles of ferromagnet that have giant magnetic moments, materials with meta magnetic transitions (first order transition from Pauli paramagnet to intinerant electron ferromagnet). If time permits we will revisit such transitions. They are already beginning to be used and some commercial machines are appearing.

Chapter 3

Magnetism of conduction electrons

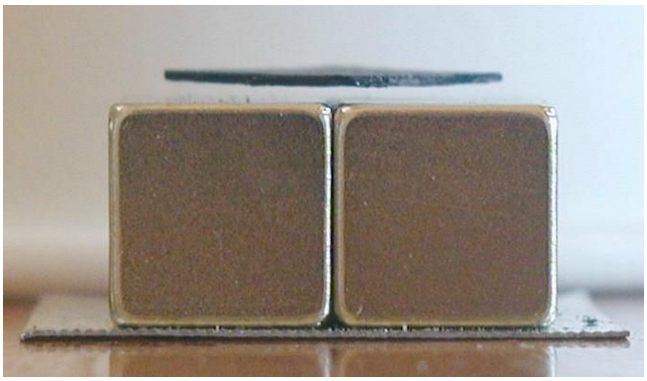

Magnetic levitation of graphite

https://sci-toys.com/scitoys/scitoys/magnets/pyrolytic_graphite.html

In the previous chapter, the focus has been on the paramagnetism of insulators including magnetic ions. The magnetism that appears due to the phase transition caused by the interaction between electron spins will be investigated in the following chapters. Here we have a short look on the magnetism of conduction electrons other than such cooperative phenomena.

3.1 Pauli paramagnetism

3.1.1 Conduction electrons

Electronic states in crystals are described by energy bands separated by energy gaps on the energy axis due to discrete spatial translational symmetry. In a system of free electrons, due to the fermionic constraint, there exists the Fermi level determined by the number of particles and the band structure. The orbital states described by Bloch functions have up-down spin degeneracy at zero field. In metals, the Fermi levels place inside energy bands (conduction bands), and we measure the Fermi energy E_{F} from the bottom of conduction band. At room temperatures $E_{\mathrm{F}} \gg k_{\mathrm{B}}T$, and the distribution is Fermi degenerated.

In many actual metals, the electronic structures are complicated due to, e.g., multiple bands in k-space, etc. However, here, to explore the essential properties, we assume a single band with single band in the center of k-space with a single effective mass. Further we ignore the mutual electron interactions, which must exist in real systems. Such a non-interacting model well describes behavior of electrons in actual metals in most cases. This gets theoretical support from Landau's **Fermi liquid theory**[10, 11].

3.1.2 Magnetic response by electron spins

To see the response of electron spins, we write the Hamiltonian in second-quantized form as

$$\mathscr{H} = \sum_{\boldsymbol{k}\sigma} E_{\boldsymbol{k}} c^{\dagger}_{\boldsymbol{k}\sigma} c_{\boldsymbol{k}\sigma} + \frac{1}{2} g\mu_{\mathrm{B}} B \sum_{\boldsymbol{k}\sigma} \sigma c^{\dagger}_{\boldsymbol{k}\sigma} c_{\boldsymbol{k}\sigma}. \tag{3.1}$$

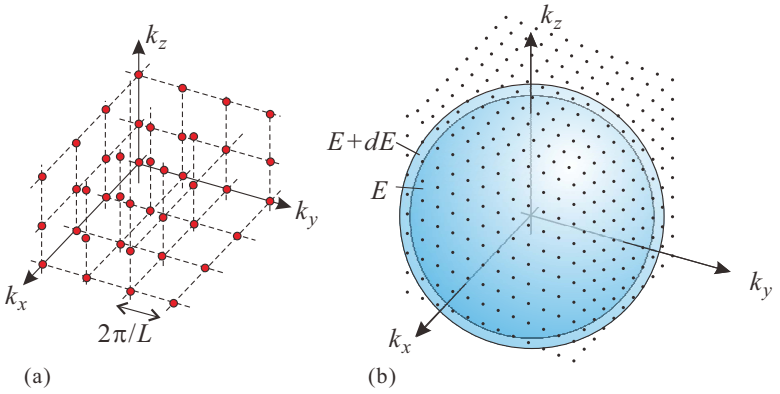

Fig. 3.1 (a) Red points represent eq. (3.2) in k-space. (b) To calculate the density of states, we count the numbe of possible points in the shell between E and $E + dE$.

$c^\dagger_{\boldsymbol{k}\sigma}$ is a creation operator of an electron with wavenumber $\boldsymbol{k}$, spin σ ($\sigma = \pm 1$ for $\uparrow\downarrow$). The first term is the kinetic energy, the second is the Zeeman energy.

We take periodic boundary condition in a cube with a side of L. $kL = 2n\pi$ (n: integer) along a side gives

$$\boldsymbol{k} = \frac{2\pi}{L}(n_x, n_y, n_z) \quad (n_x, n_y, n_z : \text{ integers}). \tag{3.2}$$

The discrete points in k-space are displayed in Fig. 3.1(a). The point density is $(L/2\pi)^3$. Let $\rho(E)$ the energy density of states per volume and per spin. ρ depends on the spin direction in ferromagnets but is common in paramagnets with time-reversal symmetry. In three dimensional free electron systems, $E_{\boldsymbol{k}} = \hbar^2 k^2/2m$ with the effective mass m. The wavenumbers which give a constant E for $E_{\boldsymbol{k}}$ are, in k-space, the points expressed in (3.2) and on the sphere with radius $k_E = \sqrt{2mE}/\hbar$. To obtain $\rho(E)$, we count such points within the shell between E and $E + dE$ and divide by dE as in Fig. 3.1(b). Thus we obtain

$$\rho(E) = \frac{1}{L^3}\left(\frac{L}{2\pi}\right)^3 4\pi k_E^2 \frac{dk_E}{dE} = \frac{1}{\pi^2\hbar^3}\sqrt{\frac{mE}{2}}. \tag{3.3}$$

The expectation value of the magnetic moment is given by

$$-\frac{g\mu_{\rm B}}{2}\sum_{\boldsymbol{k}\sigma}\sigma\left\langle c^\dagger_{\boldsymbol{k}\sigma}c_{\boldsymbol{k}\sigma}\right\rangle = \frac{g\mu_{\rm B}}{2}\sum_{\boldsymbol{k}}\left[f\left(E_{\boldsymbol{k}} - \frac{g\mu_{\rm B}B}{2}\right) - f\left(E_{\boldsymbol{k}} + \frac{g\mu_{\rm B}B}{2}\right)\right], \tag{3.4}$$

where

$$f(E) = \frac{1}{\exp[(E-\mu)/k_{\rm B}T] + 1} \tag{3.5}$$

is the Fermi distribution function with μ as the chemical potential. Then the magnetization M is given by

$$M = \frac{g\mu_{\rm B}}{2}\int_0^\infty dE\rho(E)\left[f\left(E_{\boldsymbol{k}} - \frac{g\mu_{\rm B}B}{2}\right) - f\left(E_{\boldsymbol{k}} + \frac{g\mu_{\rm B}B}{2}\right)\right]. \tag{3.6}$$

To determine μ, we write the electron concentration as $N_{\rm e}$ and use

$$N_{\rm e} = \int_0^\infty dE\rho(E)\left[f\left(E_{\boldsymbol{k}} - \frac{g\mu_{\rm B}B}{2}\right) + f\left(E_{\boldsymbol{k}} + \frac{g\mu_{\rm B}B}{2}\right)\right]. \tag{3.7}$$

Thus determined μ is the Fermi energy $E_{\rm F}$ described in Sec. 3.1.1.

We then obtain the spin magnetic susceptibility of conduction electrons at $T = 0$ as

Pauli paramagnetic susceptibility

$$\chi_{\rm Pauli} = \left(\frac{g\mu_{\rm B}}{2}\right)^2 [2\rho(E_{\rm F})]. \tag{3.8}$$

The spin susceptibility of Fermi-degenerated free electrons is constant and proportional to the density of states at the Fermi level. This is called **Pauli paramagnetism**. This result holds for general complicated band structures as long as the system can be treated as a Fermi liquid.

3.2 Landau diamagnetism

As we have seen as the Bohr-van Leeuwen theorem, that a classical system of charged particles cannot have magnetism. In real systems of charged particles, even without orbital quantization by local potentials or spins, the quantization causes magnetism. Let us have a look on that.

3.2.1 Landau quantization

Landau quantization is universally observed in the systems of free charged particles under magnetic field. Particularly in two-dimensional systems, it results in an extraordinary phenomenon called quantum Hall effect. Here we study its effect on orbital magnetism. We directly treat the orbital motions and write the Hamiltonian as

$$\mathscr{H} = \frac{1}{2m}\sum_i (\boldsymbol{p}_i + e\boldsymbol{A})^2. \tag{3.9}$$

We take Landau gauge $\boldsymbol{A} = (0, Bx, 0)$ to express the magnetic field B along z-axis. m is the electron rest mass. Schrödinger equation for a single electron is

$$-\frac{\hbar^2}{2m}\left[\frac{\partial^2}{\partial x^2} + \frac{\partial^2}{\partial z^2} + \left(\frac{\partial}{\partial y} - i\frac{eB}{\hbar}x\right)^2\right]\psi = E\psi. \tag{3.10}$$

The coordinate operator in the lhs of (3.10) is only x. Thus we assume plane wave along y and z, namely $\psi = \exp[i(k_y y + k_z z)]u(x)$. By substituting this to (3.10), we obtaine

$$-\frac{\hbar^2}{2m}\left[\frac{d^2u}{dx^2} + \left(k_y - \frac{eB}{\hbar}x\right)^2 u\right] = \left(E - \frac{\hbar^2 k_z^2}{2m}\right)u. \tag{3.11}$$

This is in the form of one-dimensional harmonic oscillator with the center coordinate

$$x_\mathrm{c} = \hbar k_y / eB. \tag{3.12}$$

The frequency of oscillator ω_c is

$$\frac{m\omega_\mathrm{c}^2}{2} = \frac{(eB)^2}{2m} \quad \therefore\ \omega_\mathrm{c} = \frac{eB}{m}. \tag{3.13}$$

This is called **cyclotron frequency**. The energy eigenvalues are

$$E(n, k_z) = \frac{\hbar^2 k_z^2}{2m} + \left(n + \frac{1}{2}\right)\hbar\omega_\mathrm{c} = \frac{\hbar^2 k_z^2}{2m} + (2n+1)\mu_\mathrm{B}B \quad (n = 0, 1, 2, \cdots). \tag{3.14}$$

The motion along z-axis is free-electron like but in xy-plane the kinetic energy is discretely quantized. This is called **Landau quantization**. The energy levels of harmonic oscillator indexed by n in (3.14) are called Landau levels.

It seems a bit strange that the solutions are strongly anisotropic although the system is uniform in xy-plane. This is the result of selection of Landau gauge to solve the equation. The symmetrically localized solutions can be obtained, e.g. by taking the symmetric gauge. These are degenerated for the same n, and with superpositions we can have eigenstates with various distributions in xy-plane. In semi-classical approach, the Landau quantization can be viewed as the quantization of cyclotron motion through the spatial localization. However there still exists the freedom in taking the center of cyclotron motion, that gives large degree of degeneracy and results in the eigenstates with various outlook.

3.2.2 Orbital diamagnetism

We consider the normalization of eigenstates in the form of $\exp[i(k_y y + k_z z)]u(x)$ in the cube with side length L. z-direction is the same as free electrons. From $k_z = (2\pi/L)n_z$ ($n_z = 0, \pm 1, \cdots$), $E_z = \hbar^2 k_z^2/2m$, possible number of k_z for kinetic energy along z-direction less than E_z is $2L\sqrt{2mE_z}/h$. Also for y, because the form is plane wave, from the periodic boundary condition

$$k_y = \frac{2\pi}{L} n_y \quad (n_y = 0, \pm 1, \pm 2, \cdots). \tag{3.15}$$

On the other hand, k_y relates with the center x_c of harmonic oscillator along x-direction as (3.12), then when x_c is in the region $[-L/2, L/2]$,

$$-\frac{L}{2} \le \frac{\hbar}{eB} k_y = \frac{\hbar}{eB}\frac{2\pi}{L} n_y \le \frac{L}{2} \quad \therefore\ |n_y| \le \frac{eBL^2}{4\pi\hbar}.$$

This means the degree of degeneracy of a single Landau level in xy-plane is eBL^2/h.

From the above, $\Omega(E)$, the number of states below the total energy E is

$$\Omega(E) = \frac{L^3}{\hbar^2}\sqrt{8m}eB \sum_{n=0}^{n_\mathrm{max}} \sqrt{E - (2n+1)\mu_\mathrm{B}B}, \tag{3.16}$$

where

$$n_\mathrm{max} = \mathrm{int}\left(\frac{E - \mu_\mathrm{B}B}{2}\right). \tag{3.17}$$

Because the density of states is given by $d\Omega/dE$, the Free energy of the system is

$$F = N\mu - 2k_\mathrm{B}T \int \frac{d\Omega}{dE} \ln\{1 + \exp[-(E-\mu)/k_\mathrm{B}T]\} dE, \tag{3.18}$$

where we consider the spin degree of freedom 2. The integral part is partially integrated as follows.

$$\begin{aligned}
\int \frac{d\Omega}{dE} \ln\{1 + \exp[-(E-\mu)/k_\mathrm{B}T]\} dE &= -\int \Omega(E) \left(-\frac{1}{k_\mathrm{B}T}\right) \frac{\exp[-(E-\mu)/k_\mathrm{B}T]}{1 + \exp[-(E-\mu)/k_\mathrm{B}T]} dE \\
&= \frac{1}{k_\mathrm{B}T} \int \left[\int \Omega(E) dE\right] \frac{d}{dE} \frac{1}{1 + \exp[(E-\mu)/k_\mathrm{B}T]} dE \\
&= \frac{1}{k_\mathrm{B}T} \frac{2\sqrt{8m}}{3} \frac{eBL^3}{h^2} \int \sum_{n=0}^{n_\mathrm{max}} [E - (2n+1)\mu_\mathrm{B}B]^{3/2} \frac{d}{dE} \frac{1}{1 + \exp[(E-\mu)/k_\mathrm{B}T]} dE.
\end{aligned}$$

From $\mu_\mathrm{B} = e\hbar/2m$ we can rewrite F as

$$F = N_\mathrm{e}\mu - A \int \phi(E) \frac{d}{dE} \frac{1}{1 + \exp[(E-\mu)/k_\mathrm{B}T]} dE, \tag{3.19a}$$

where

$$A = \frac{16L^3}{3\pi^2\hbar^3} m^{3/2} (\mu_\mathrm{B}B)^{5/2}, \tag{3.19b}$$

$$\phi(E) = \sum_{n=0}^{n_\mathrm{max}} \left[\frac{E}{2\mu_\mathrm{B}B} - \left(n + \frac{1}{2}\right)\right]^{3/2}. \tag{3.19c}$$

Taking the limit $B \to 0$, it becomes

$$F = N_\mathrm{e}E_\mathrm{F} - A\phi(E_\mathrm{F}). \tag{3.20}$$

Here we use the asymptotic form for $x \gg 1$

$$\sum_{n=0}^{n_\mathrm{max}} \left[x - \left(n + \frac{1}{2}\right)\right]^{3/2} \approx \frac{2}{5}x^{5/2} - \frac{1}{16}x^{1/2} + \cdots. \tag{3.21}$$

This is obtained by applying the Euler–Maclaurin formula to $F(y) = (x-y)^{3/2}$ as follows.

$$\sum_{n=0}^{n_0} F(n+1/2) \approx \int_0^{n_0+1} dy F(y) - \frac{1}{24}[F'(n_0+1) - F'(0)]$$
$$\approx \frac{2}{5}x^{5/2} - \frac{1}{16}x^{1/2}.$$

Hence we obtain the asymptotic expansion

$$\phi(E) = \frac{2}{5}\left(\frac{E}{2\mu_{\rm B}B}\right)^{5/2} + \frac{1}{16}\left(\frac{E}{2\mu_{\rm B}B}\right)^{1/2} + \cdots, \tag{3.22}$$

which gives the free energy as

$$F = \text{const.} - \frac{L^3}{3}\rho(E_{\rm F})(\mu_{\rm B}B)^2 + \cdots. \tag{3.23}$$

Then we obtain the orbital diamagnetic susceptibility of free electrons as

Landau diamagnetic susceptibility

$$\chi_{\rm Landau} = -\frac{2}{3}\rho(E_{\rm F})\mu_{\rm B}^2. \tag{3.24}$$

This is called **Landau diamagnetism**.

Taking the effective mass to the free electron rest mas, $\chi_{\rm Landau}$ has the opposite sign to $\chi_{\rm Pauli}$ and the magnitude is 1/3. The total susceptibility is then

$$\chi = \chi_{\rm Pauli} + \chi_{\rm Landau} = \frac{4}{3}\rho(E_{\rm F})\mu_{\rm B}^2. \tag{3.25}$$

Appendix 5A: Weak crystal field approximation

In the lecture on $3d$ transition metal ions, we consider the approximation of a strong crystal field (ligand field), that is, the one-electron states of $3d$ electron in the crystal field are considered first, and fill them with electrons to consider multi-electron states. On the other hand, there is also a method that first assumes the LS multiplex term as we did in the case of $4f$ lanthanoid ion, and then considers how this multi-electronic state splits in the crystal field using point group theory. This is called **weak crystal field approximation**. In Fig. 5A.1, we show how the state d^n splits in an octahedral potential.

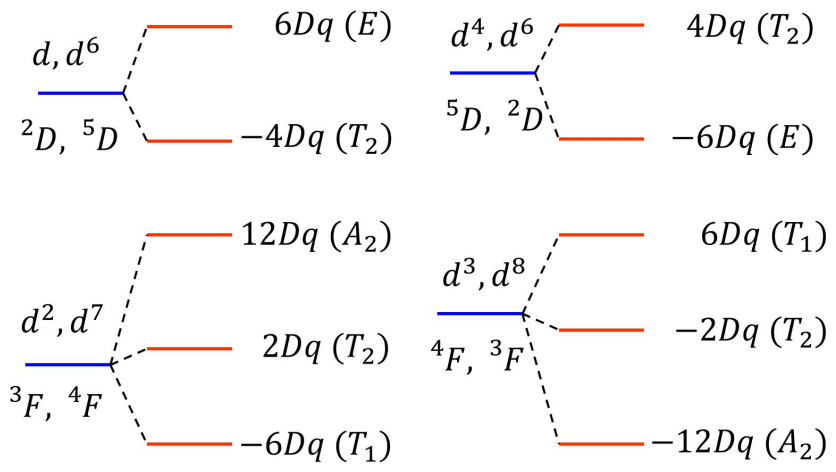

Fig. 5A.1 Split of d^n state in an octahedral crystal potential in weak crystal field approximation.

References

[1] Charles P. Slichter. *Principles of Magnetic Resonance (Springer Series in Solid-State Sciences) by Charles P. Slichter(2010-12-01)*. Springer, 1653.

[2] Marcus A. Hemminga and Lawrence Berliner. *ESR Spectroscopy in Membrane Biophysics (Biological Magnetic Resonance Book 27) (English Edition)*. Springer, 8 2007.

[3] M. H. L. Pryce. *Proc. Phys. Soc.*, Vol. A63, p. 25, 1950.

[4] Mohammad Mostafanejad. Basics of the spin hamiltonian formalism. *International Journal of Quantum Chemistry*, Vol. 114, No. 22, pp. 1495–1512, June 2014.

[5] 上村洸, 菅野暁, 田辺行人. 配位子場理論とその応用 (物理科学選書). 裳華房, 6 1969.

[6] Sundar R. Bairavarasu, Matthew E. Edwards, Medury D. Sastry, Tatiana Kukhtareva, Holger M. Jaenisch, Rastgo H. Hawrami, Dimitrios Lianos, and Manmohan D. Aggarwal. Photo-EPR studies of photorefractive batio$_3$ heavily doped with cr^{3+}: evidence of photo-induced dissociation of cr^{3+} dimers. In Ruyan Guo, Shizhuo S. Yin, and Francis T. S. Yu, editors, *Photonic Fiber and Crystal Devices: Advances in Materials and Innovations in Device Applications*. SPIE, September 2007.

[7] R Böttcher, E Erdem, H T Langhammer, T Müller, and H-P Abicht. Incorporation of chromium into hexagonal barium titanate: an electron paramagnetic resonance study. *Journal of Physics: Condensed Matter*, Vol. 17, No. 17, pp. 2763–2774, April 2005.

[8] O. V. Lounasmaa. *Experimental Principles and Methods Below 1K*. Academic Pr, 6 1974.

[9] Koji Kamiya, Koichi Matsumoto, Takenori Numazawa, Shinji Masuyama, Hiroyuki Takeya, Akiko T. Saito, Naoya Kumazawa, Kazumi Futatsuka, Keigo Matsunaga, Tsuyoshi Shirai, Suguru Takada, and Teruhito Iida. Active magnetic regenerative refrigeration using superconducting solenoid for hydrogen liquefaction. *Applied Physics Express*, Vol. 15, No. 5, p. 053001, January 2022.

[10] L. D. Landau. The theory of a fermi liquid. *Sov. Phys. JETP*, Vol. 3, pp. 920–925, 1957.

[11] Piers Coleman. *Introduction to Many-Body Physics*. Cambridge University Press, 11 2015.